Bioorganic & Medicinal Chemistry 17 (2009) 6631–6640

Contents lists available at ScienceDirect

Bioorganic & Medicinal Chemistry

journal homepage: www.elsevier.com/locate/bmc

Evaluation of delocalized lipophilic cationic dyes as delivery vehicles for photosensitizers to mitochondria

Ethel J. Ngen, Pallavi Rajaputra, Youngjae You *

Department of Chemistry and Biochemistry, South Dakota State University, Brookings, SD 57007, USA

ARTICLE INFO

Article history:
Received 22 June 2009
Revised 25 July 2009
Accepted 28 July 2009
Available online 3 August 2009

Keywords:
Mitochondria targeting
Delocalized lipophilic cationic dyes
Photodynamic therapy
Anticancer therapy

ABSTRACT

Mitochondria are attractive targets in photodynamic therapy. Two conjugates: TPP–Rh (a porphyrin–rhodamine B conjugate) and TPP–AO (a porphyrin–acridine orange conjugate), each possessing a single delocalized lipophilic cation, were designed and synthesized as photosensitizers. Their ability to target the mitochondria for photodynamic therapy was evaluated. The conjugates were synthesized by conjugating a monohydroxy porphyrin (TPP-OH) to rhodamine B (Rh B) and acridine orange base (AO), respectively, via a saturated hydrocarbon linker. To evaluate the efficiency of the conjugates as photosensitizers, their photophysical properties and in vitro photodynamic activities were studied in comparison to those of TPP-OH. Although fluorescence energy transfer (FRET) was observed in the conjugates, they were capable of generating singlet oxygen at rates comparable to TPP-OH. Biologically, exciting results were observed with TPP–Rh, which showed a much higher phototoxicity [IC_{50}, 3.95 μM: irradiation of 400–850 nm light (3 mW cm^{-2}) for 1 h] than either TPP-OH or Rh B (both, IC_{50}, >20 μM) without significant dark toxicity at 20 μM. This improved photodynamic activity might be due to a greater cellular uptake and preferential localization in mitochondria. The cellular uptake of TPP–Rh was 8 and 14 times greater than TPP-OH and Rh B, respectively. In addition, fluorescence imaging studies suggest that TPP–Rh localized more in mitochondria than TPP-OH. On the other hand, TPP–AO showed some dark toxicity at 10 μM and stained both mitochondria and nucleus. Our study suggests that conjugation of photosensitizers to Rh might provide two benefits, higher cellular uptake and mitochondrial localization, which are two important subjects in photodynamic therapy.

1. Introduction

Photodynamic therapy (PDT) is a recently approved clinical modality used in treating cancers. PDT has great potential in eliminating severe side effects characteristic of conventional chemotherapies and radiation therapies.[1–5] PDT involves three main components: a photosensitizer, molecular oxygen, and light. Cytotoxic effects in PDT are driven by reactive oxygen species, prevalently singlet oxygen, which are generated in biological systems from tissue oxygen upon activation of a photosensitizer with light of an appropriate wavelength.[6–9] Singlet oxygen tends to have a very short lifetime in biological systems (<0.04 μs) and consequently a very short radius of action (<0.02 μm).[6–8] As a result, the site of localization of the photosensitizer is often the site of initial photodamage.[9,10]

Mitochondria are very attractive sites for the localization of photosensitizers in PDT since they play an integral role in various cell biology processes such as energy production, apoptotic cell death, molecular metabolism, calcium signaling, and cell redox status.[11–13] Furthermore, mitochondrial photodamage has been reported to be the major cause of apoptosis induction in PDT.[9,12–15] Although lysosomal photodamage has also been reported to induce apoptosis in PDT, this phenomenon has been attributed to either the relocalization of the photosensitizers to mitochondria or the destabilization of the mitochondria after irradiation.[9,10,16,17] Consequently a number of photosensitizers have been designed to target the mitochondria for improved PDT efficiency.[17]

In this report, we describe the syntheses, photophysical characterization, and in vitro photodynamic studies of two conjugates: TPP–Rh (a porphyrin–rhodamine B conjugate) and TPP–AO (a porphyrin–acridine orange conjugate), each possessing a single delocalized lipophilic cation for mitochondria targeting (Fig. 1). We envisioned that by conjugating a monohydroxy porphyrin (TPP-OH) to rhodamine B (Rh B) and acridine orange base (AO), respectively, via a saturated hydrocarbon linker, we could get the conjugates to preferentially accumulate in the mitochondria, ultimately improving the PDT efficiency. To evaluate the efficiency of the conjugates as photosensitizers we studied both their photophysical properties and in vitro photodynamic activities in comparison to those of their individual components.

* Corresponding author. Tel.: +1 605 688 6905; fax: +1 605 688 6364.
E-mail address: youngjae.you@sdstate.edu (Y. You).

0968-0896/$ - see front matter © 2009 Elsevier Ltd. All rights reserved.
doi:10.1016/j.bmc.2009.07.074

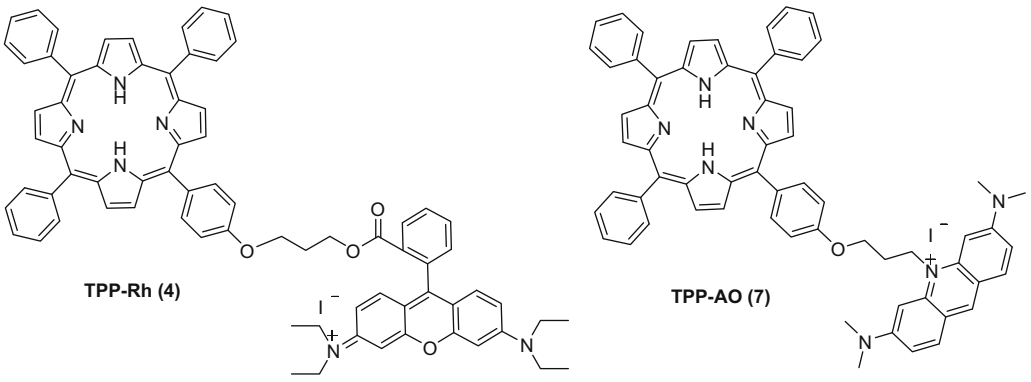

Figure 1. Structures of conjugates.

2. Results and discussion

2.1. Chemistry

Two conjugates, TPP–Rh (**4**) and TPP–AO (**7**), both containing delocalized lipophilic cations were synthesized (Scheme 1) and their ability to target the mitochondria was evaluated. Both conjugates were designed to possess delocalized lipophilic cations in order to facilitate their accumulation in mitochondria, by exploiting the mitochondrial membrane potential difference. Rh B was chosen because it possesses a delocalized positive charge and could be easily tethered to TPP-OH by esterification. AO on the other hand was chosen because it could be easily conjugated to TPP-OH by alkylation thus forming a quaternary amine, similar to nonyl acridine orange which possesses a quaternary amine and has been shown to preferential accumulate in the mitochondria.[11] Derivatives of both rhodamine and acridine orange dyes, such as Rh 123 and nonyl-AO, have been shown to specifically accumulate in the mitochondria by exploiting the mitochondrial membrane potential difference.[11,18]Although both conjugates were synthesized from TPP-OH, the procedures differed slightly.

2.1.1. Syntheses of TPP–Rh (4) and TPP–AO (7) conjugates

For TPP–Rh **(4)** TPP-OH was first reacted with 1,3-dibromopropane in acetone under reflux to give 5,10,15-triphenyl-20-(3-bromopropyl phenyl ether)-21*H*,23*H*-porphyrin **(3)**. This was then conjugated to Rh B under reflux to afford the pure final product in 51% yield. However, for TPP–AO **(7)** because compound **3** was unable to react with acridine orange, 1,3-dibromopropane was first converted to 1,3-diiodopropane **(5)**, then reacted with TPP-OH. The 5,10,15-triphenyl-20-(3-iodopropyl phenyl ether)-21*H*,23*H*-porphyrin **(6)** was next reacted with acridine orange base in a toluene/dimethylformamide mixture under reflux to give the pure final product in 54% yield. This difference was probably due to iodine's ability to act as a better leaving group. Despite this, both conjugation reactions took several days, probably due to steric hindrance in the dyes and their high lipophilicity. Moderate yields were obtained for both conjugation reactions: 51% and 54% for TPP–Rh and TPP–AO, respectively.

2.2. Photophysical properties

2.2.1. Absorption spectra and molar extinction coefficients

Both conjugates contained all the characteristic absorption peaks of their respective components (Fig. 2), indicating that no significant electronic interactions might occur in the ground state.[19] However, whereas the Soret band of TPP–Rh remained practically the same as that in TPP-OH, the Soret band of TPP–AO had a much lower molar extinction coefficient (Table 1). Thus it might indicate some degree of aggregation in the ground state.[20] Furthermore, in both conjugates there was a slight red shift of Rh B and AO peaks from 550 to 560 nm and from 490 to 506 nm, respectively. This shift was not however observed in equimolar mixtures of TPP-OH + Rh B and TPP-OH + AO (Fig. 2). This might be due to the proximity of the TPP moiety which seemed to change the polarity of the environment, consequently red shifting the maxima of both Rh B and AO in the respective conjugates.[21,22]

2.2.2. *n*-Octanol/pH 7.4 buffer partition coefficients

TPP–Rh was most lipophilic, followed by Rh B, then TPP-OH, TPP–AO and finally AO·HCl (Table 1). The lipophilicity of the conjugates differed from each other (log $D_{7.4}$, 3.53 for TPP–Rh and 0.79 for TPP–AO) and was approximately the sum of the lipophilicity of their individual components.

2.2.3. Aggregation tendency of the dyes

Generally, the tendency for dyes to aggregate is greatly dependent on both their lipophilicity and their molecular structure.[20] Aggregation usually leads to a decrease in the quantum yields for photophysical processes such as fluorescence emission and singlet oxygen generation, consequently decreasing the photodynamic activity of photosensitizers.[23] The aggregation tendency in media could be translated to that in the cytoplasm and consequently it could cause reduced phototoxicity. Although the lipophilicity of the conjugates seemed to differ from each other and from that of TPP-OH, their aggregation tendencies in aqueous complete media were similar (Fig. 3). They all aggregate more in aqueous media and less in DMSO. This suggests that their aggregation tendencies could be attributed mostly to their highly planar structures. Rh B, however, showed an unusual aggregation trend, aggregating more in DMSO and less in aqueous media. This is probably due to the presence of the unsaturated bond which permits free rotation of the carboxyl phenyl ring thus facilitating its solubility in aqueous media.

2.2.4. FRET in the conjugates

The 3D fluorescence scans showed efficient FRET from the Rh and AO moieties to the TPP moieties in the respective conjugates (Fig. 4). However, no FRET was observed in equimolar mixtures of the respective conjugate components. This could be attributed to the proximity of the dyes in the conjugates and is supported by no FRET in the equimolar mixtures of the respective conjugate components where the dyes can freely move around.

2.2.5. Singlet oxygen generation

The rates of DPBF oxidation by both conjugates were similar to that by TPP-OH (Fig. 5). This indicates that although FRET was observed in both conjugates, they were able to generate singlet oxygen at rates comparable to that of TPP-OH. However, DPBF was not oxi-

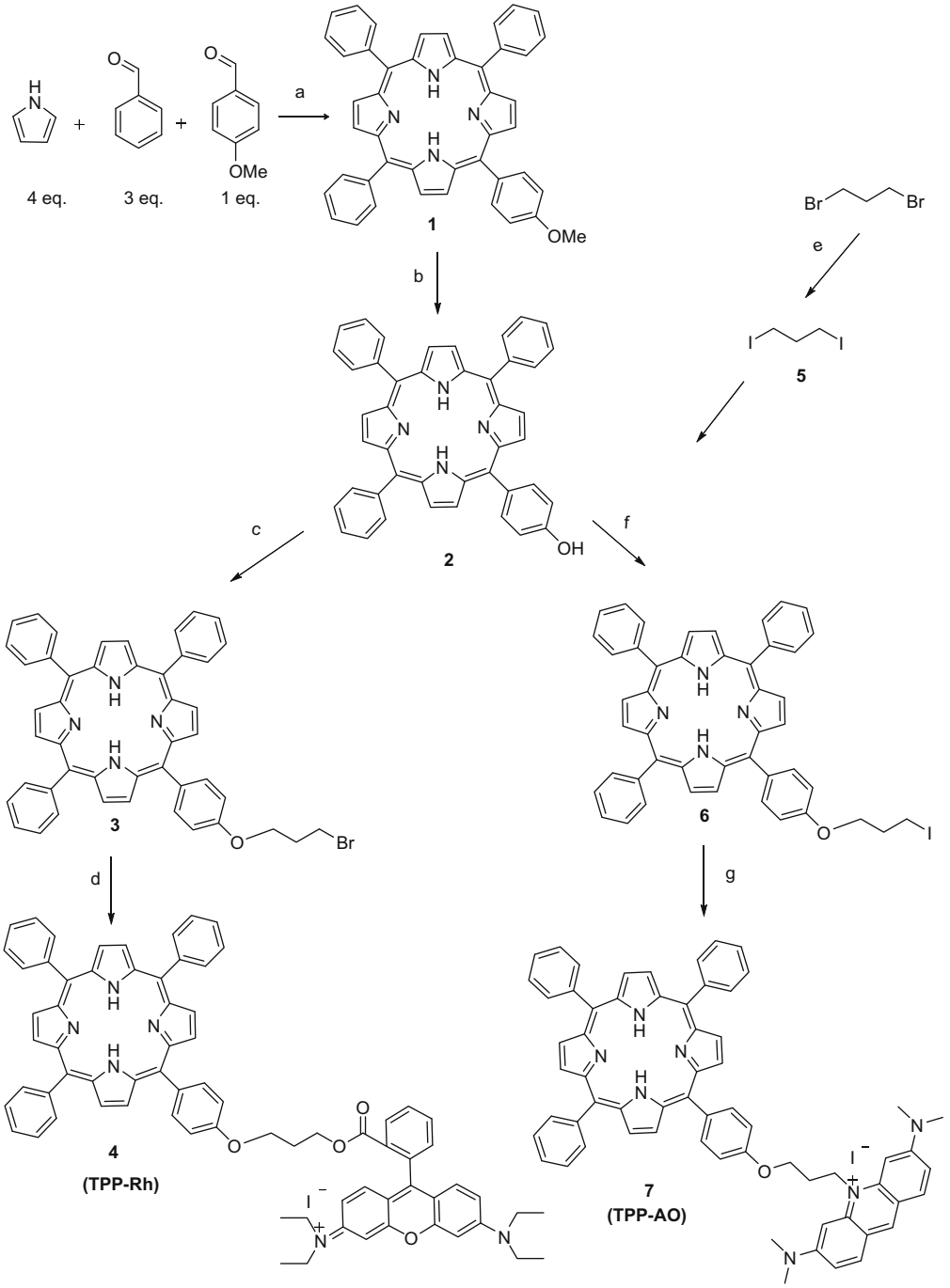

Scheme 1. Reagents: (a) (i) 0.08 equiv $BF_3{\cdot}Et_2O$, (ii) 3.6 equiv TFA, (iii) 3 equiv DDQ, dichloromethane; (b) (i) 2 equiv BBr_3, dichloromethane; (c) (i) 10 equiv $BrCH_2CH_2CH_2Br$, (ii) 10 equiv K_2CO_3, acetone; (d) (i) 20 equiv K_2CO_3, (ii) 20 equiv KI, (iii) 10 equiv Rhodamine B, acetone; (e) (i) 6 equiv KI, acetone; (f) (i) 5 equiv K_2CO_3, acetone; (g) (i) 1 equiv acridine orange base, dimethylformamide, toluene.

dized by either Rh B or AO·HCl under the same irradiation conditions. The rates of DPBF oxidation were calculated from the time of initial irradiation (2–10 min) since a slight increase in absorbance was noticed from all samples upon initial irradiation (from 0 to 2 min). This increase could be attributed to an increase in temperature (~4 °C) which then led to an increase in DPBF's solubility in methanol.

2.3. Biological studies

2.3.1. Intracellular accumulation

Despite their larger sizes, the conjugates were more accumulated within cells than the unconjugated dyes (Fig. 6). TPP–AO showed the greatest intracellular accumulation [about 12 times that of TPP-OH (68.2 vs 5.6 fmol/cell)] followed by TPP–Rh with an intracellular accumulation about 8 times that of TPP-OH (44.0 vs 5.6 fmol/cell), then AO·HCl. The uptake of TPP-OH and Rh B was less than 10 fmol/cell. The higher accumulation of the conjugates compared to the unconjugated dyes could be attributed to the delocalized positive charge on the molecules and their increased flexibility by the aliphatic linker. The delocalized positive charge on the molecules might facilitate binding to negatively charged proteoglycan on cell membrane and diffusion into the cells and the mitochondria against the potential gradient.[15,17,18,24] The increased flexibility of the conjugate might contribute to the

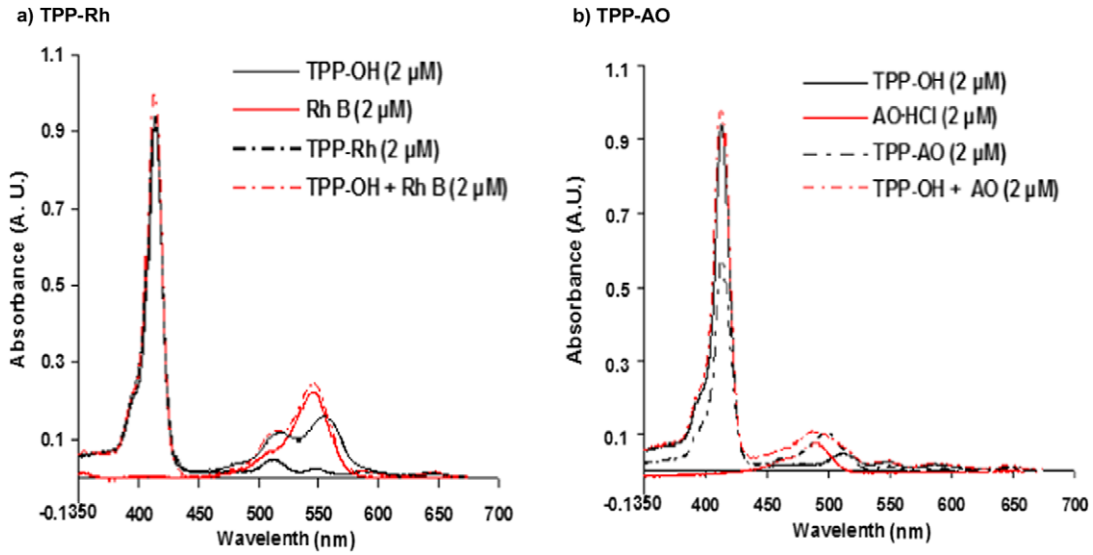

Figure 2. (a) The absorption spectra of TPP–Rh (2 μM); its components (TPP-OH (2 μM), Rh B (2 μM)) and an equimolar mixture of its components (TPP-OH + Rh B (2 μM)) in methanol. (b) Absorption spectra of TPP–AO (2 μM); its components (TPP-OH (2 μM), AO·HCl (2 μM)) and an equimolar mixture of its components (TPP-OH + AO·HCl (2 μM)) in methanol.

Table 1
UV–vis-near-IR band maxima and molar absorptivities in dichloromethane[a] and *n*-octanol/pH 7.4 buffer partition coefficients of dyes

Compds	Soret band	Band IV	Band III	Band II	Band I	Log $D_{7.4}$
TPP–OH	419 (405)	517 (14.7)	552 (7.4)	593 (4.5)	649 (4.3)	2.30
TPP–Rh	419 (389)	522 (37.4)	562 (50.1)		649 (4.7)	3.53
TPP–AO	419 (304)	506 (48.2)	553 (7.1)	593 (4.1)	649 (3.7)	0.79
Rh B			550 (60.6)			2.20
AO·HCl[b]		490 (82.3)				-0.99

[a] $\lambda_{max,}$ nm ($\varepsilon \times 10^3$ M^{-1} cm^{-1}).
[b] AO·HCl in ethanol.

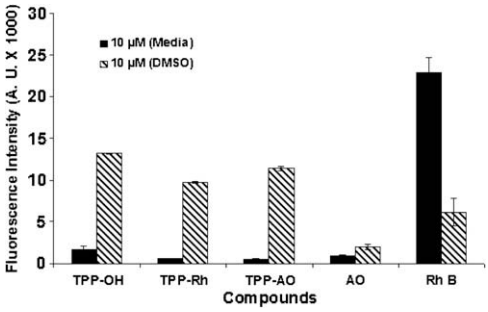

Figure 3. Fluorescence emission from the respective dyes (10 μM) in both complete media and DMSO. Whereas TPP-OH, TPP–Rh and TPP–AO were excited at 420 nm and the fluorescence read at 650 nm, the following excitation and emission wavelengths were used for Rh B (Ex: 550 nm, Em: 580 nm) and AO·HCl (Ex: 430 nm, Em: 530 nm). Each data point represents the average from three separate experiments, error bars are SEM.

enhanced uptake at least in part by increasing the entropy of the conjugates.[25]

2.3.2. Stability of the ester group of TPP–Rh in cells

Since ester bonds can be cleaved in cells, the stability of the ester bond of TPP–Rh was determined. Signature of fluorescence peaks of TPP–Rh was used. The fluorescence spectrum of TPP–Rh in the cell lysate was similar to that of TPP–Rh in DMSO and different from that of an equimolar mixture of TPP-OH and Rh B in DMSO (Fig. 7). In addition, the ratio of the integral of the fluorescence peak at 580 nm to that at 650 nm of TPP–Rh in the cell lysate was similar to that of TPP–Rh in DMSO. A ratio of 0.25 was obtained for TPP–Rh in the cell lysate and 0.21 for TPP–Rh in DMSO. This indicates that the ester bond might not be cleaved in cells unless both cleaved products, TPP and Rh B derivatives, are cleared from the cell immediately. This is probably due to steric hindrance in the conjugate. Consequently, it can be inferred that TPP–Rh, acted as the conjugate once delivered to the cells.

2.3.3. Sub-cellular localization

As detailed in Section 4, dual staining of each dye with MG (MitoTracker Green) was first tried to determine localization in mitochondria. The dual staining of TPP–Rh with MG was successful. However, TPP-OH and TPP–AO dual staining with MG was not possible due to the overlapping fluorescence of TPP-OH and TPP–AO with MG. Whereas, for cells stained with 1 μM MG, exposure times of 37 ms and 5 s were required for the green and red filter, respectively, the following exposure times were required for the other dyes using the green and red filters, respectively: 2 μM TPP-OH (5 s and 5 s), 5 μM TPP–Rh (4.5 s and 330 ms), and 2 μM TPP–AO (40 ms and 2 s). In the dual staining of TPP–Rh with MG, the green and red filter could capture fluorescence from MG and TPP–Rh, respectively. Exposure times of 23 ms and 230 ms were needed for the green and red filter, respectively, which are close to the time scales for taking an image from individual staining with each filter. Since dual staining was not successful for TPP-OH and TPP–AO with MG, fluorescence images of individual staining were used to assess the sub-cellular localization.

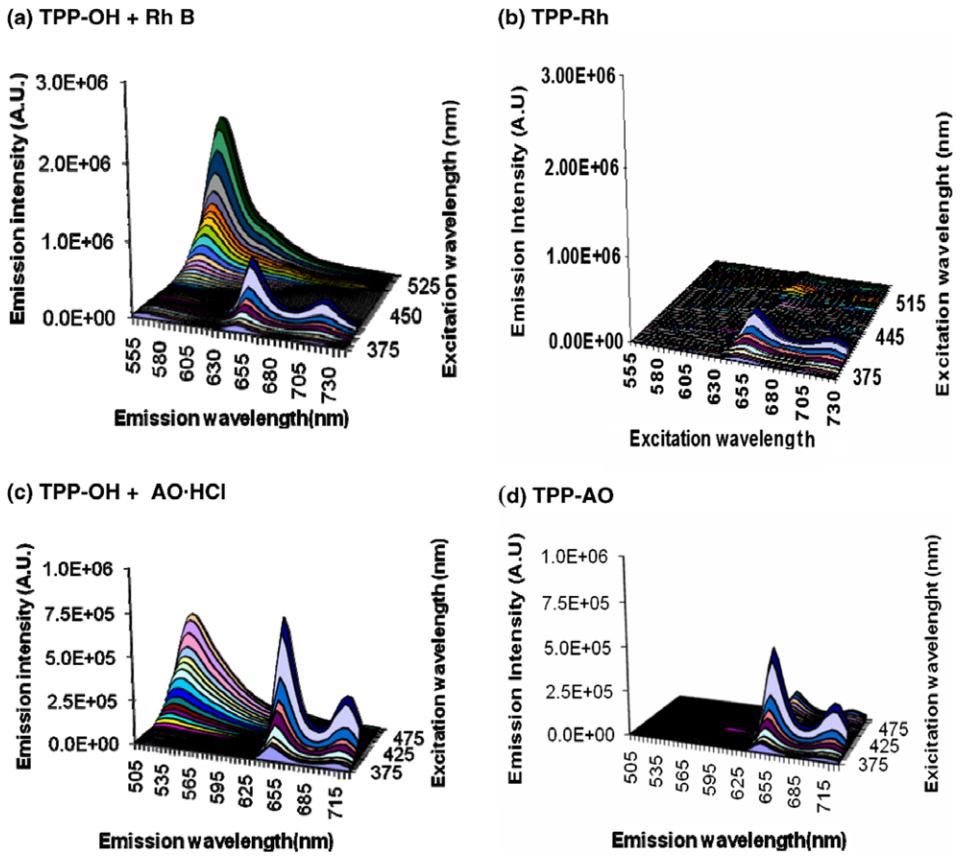

Figure 4. 3D fluorescence scans of (a) TPP-OH + Rh B (1 μM), (b) TPP–Rh (1 μM), (c) TPP-OH + AO·HCl (1 μM), (d) TPP–AO (1 μM). Whereas (a) and (b) were excited at 550 nm and the fluorescence read from 555 to 750 nm, (c) and (d) were excited at 500 nm and the fluorescence read from 505 nm to 750 nm.

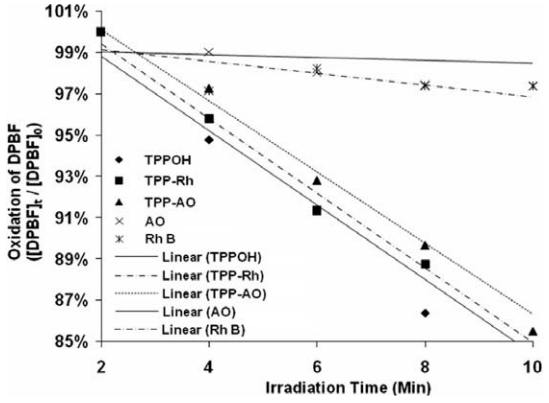

Figure 5. Relative rates of oxidation of DPBF by singlet oxygen generated from the respective dyes irradiated with a 60 W halogen lamp at 0.5 mW cm^{-2}. Five micrometers of the respective dyes were mixed with 100 μM of DPBF and the mixture irradiated for 10 min. Absorbance readings were taken every 2 min from 2 to 10 min. Each data point represents the average from three separate experiments, error bars were omitted for clarity.

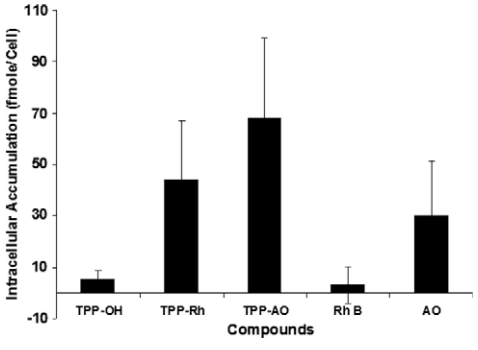

Figure 6. Intracellular accumulation of dyes in R3230AC cells. Cells were incubated with the respective dyes (10 μM) for 24 h and the intracellular uptake determined from a fluorescence calibration curve. Each data point represents the average from three separate experiments, error bars are the SEM.

Both TPP–Rh and TPP–AO showed a different localization pattern from that of TPP-OH (Fig. 8). Whereas TPP-OH seemed to have been accumulated in localized vesicles in the peri-nuclear area (Fig. 8b), TPP–Rh was distributed throughout the cytoplasm like MG (Fig. 8d–f). However, TPP–AO showed two differences in pattern compared to TPP–Rh and MG (not shown). Staining of TPP–AO was more homogeneous throughout cytosol and also stained nucleus, presumably due to interactions with cytosolic RNAs and nuclear DNA. In contrast, TPP–Rh and MG showed punctuate staining patterns consistent with mitochondrial localization. TPP–Rh showed a very similar staining pattern to MG. This sub-cellular localization of TPP–Rh was further confirmed by the dual staining studies. From the image analysis of the superimposed MG (green filter) and TPP–Rh (red filter) images, the yellow regions indicate regions of colocalization (Fig. 8f). The TPP–Rh might be accumulated in mitochondria due to the presence of the delocalized lipophilic cation which permitted their accumulation in mitochondria.

2.3.4. Dark toxicity

No significant dark toxicity was observed in cells treated with up to 20 μM of either TPP–Rh, TPP-OH, or Rh B. This was probably due to their inability to generate singlet oxygen in the dark.

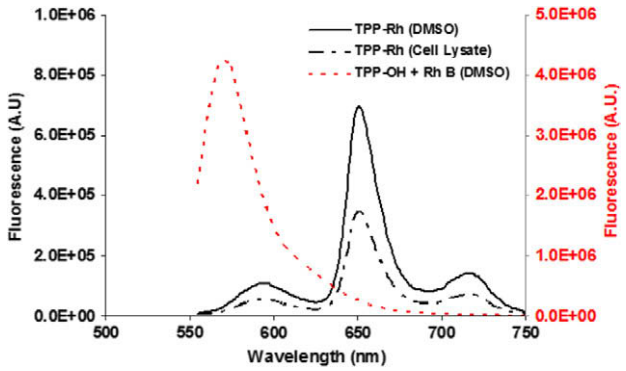

Figure 7. Stability of the ester group in TPP–Rh: fluorescence spectra of TPP–Rh and a mixture of TPP-OH and Rh B in DMSO (each 10 μM) and R3230AC cell lysate after incubated with TPP–Rh (10 μM) for 24 h. Samples were excited at 550 nm and the fluorescence read from 555 to 750 nm. Two *Y*-axis scales were used to take into account the differences in fluorescence intensities of TPP–Rh (Y1: black colored scale) and TPP-OH + Rh B (Y2: red colored scale).

However moderate dark toxicity was observed in cells treated with more than 5 μM of either AO·HCl or TPP–AO (Fig. 9). Presumably, it was caused by inherent toxic mechanisms of AO such as DNA intercalation and inhibition of protein synthesis.[26–31]

2.3.5. Phototoxicity

No significant phototoxicity was observed in cells treated with up to 20 μM of either TPP-OH or Rh B and irradiated with a 60 W halogen lamp at 3 mW cm^{-2} for an hour (Fig. 10). On the other hand, cells treated with either TPP–Rh, TPP–AO or AO·HCl and irradiated under the same conditions showed significant phototoxicity. AO·HCl showed the highest phototoxicity under the above irradiation conditions with an IC_{50} of 2.29 μM, followed by TPP–AO with an IC_{50} of 3.28 μM and then TPP–Rh with an IC_{50} of 3.95 μM. The absence of phototoxicity observed in the cells treated with up to 20 μM of either TPP-OH or Rh B could be attributed to a number of reasons. In TPP-OH this might be due to its low intracellular accumulation and formation of aggregates in aqueous media. While in Rh B this might be due to low intracellular accumulation

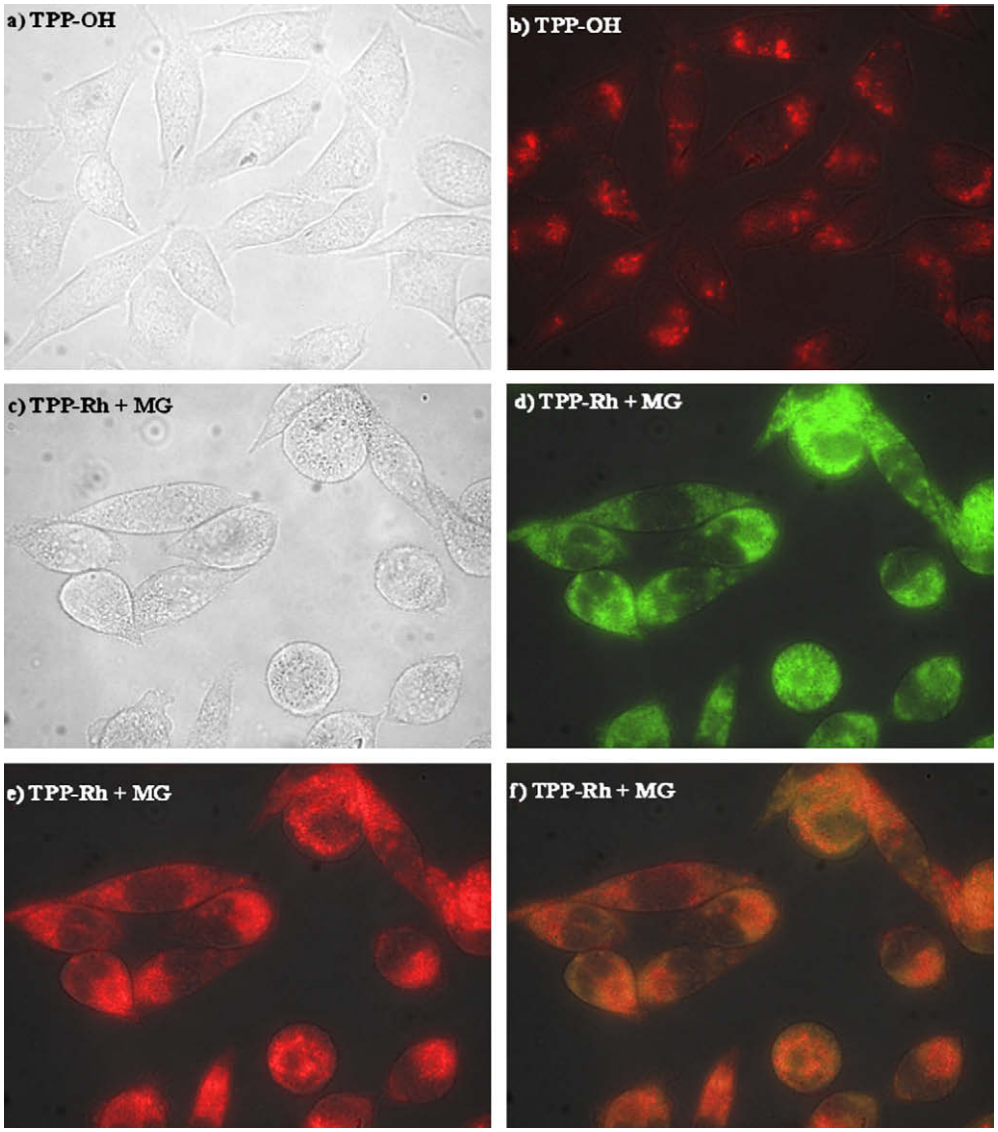

Figure 8. Sub-cellular localization of TPP-OH and TPP-conjugates: Cells treated with TPP-OH (2 μM) alone: (a) Bright field (50 ms), (b) red filter (5s); TPP–Rh (5 μM) + MG (1 μM): (c) bright field (50 ms), (d) green filter (23 ms), (e) red filter (230 ms), (f) overlap: bright field (c), green filter (d) and red filter. All images were made using R3230AC cells after incubated with dye(s) for 8 h (TPP-OH, TPP–Rh, and TPP–AO) or 1 h (MG).

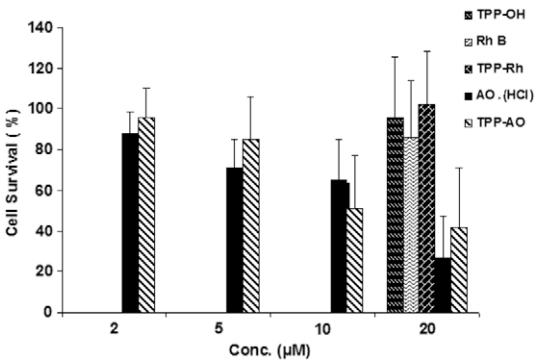

Figure 9. Dark toxicities of the respective dyes incubated in R3230AC cells for 24 h at different concentrations. Whereas TPP-OH, TPP–Rh, and Rh B were incubated at 20 μM, TPP–AO, and AO·HCl were incubated at 2 μM, 5 μM, 10 μM and 20 μM and kept in the dark. Each data point represents the average from three separate experiments, error bars are the SEM.

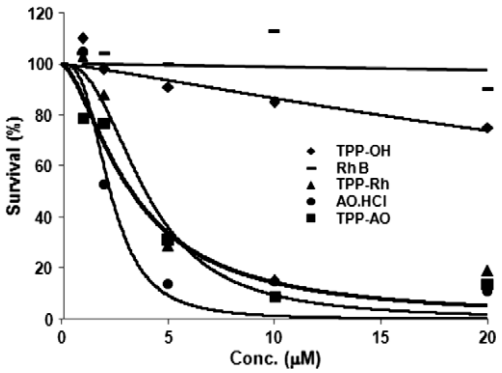

Figure 10. Phototoxicity of R3230AC cells treated with the respective dyes and irradiated with a 60 W halogen lamp at 3 mW cm^{-2} for 1 h. Cells were incubated with the respective dyes at 1, 2, 5, 10, and 20 μM, respectively, for 24 h prior to irradiation. Each data point represents the average from three separate experiments, error bars are the SEM.

and low quantum yields for singlet oxygen generation. On the other hand, the greater phototoxicity observed with TPP–Rh and TPP–AO, despite their large size, high lipophilicity, and tendency to aggregate in aqueous media, could be attributed to their high intracellular accumulation and sub-cellular localization in singlet oxygen-sensitive organelles like mitochondria. Although there was no significant generation of singlet oxygen under our experimental condition (Fig. 5), AO·HCl showed the most phototoxic effect. It might be due to the phototoxic effect via type I mechanism in addition to its dark toxicity.[32]

3. Summary and conclusions

Two conjugates, TPP–Rh and TPP–AO, were successfully synthesized by linking a monohydroxy porphyrin (TPP-OH) to rhodamine B (Rh B) and acridine orange base (AO), respectively, via a saturated hydrocarbon linker in moderate yields. Although FRET was observed in both conjugates, they were able to generate singlet oxygen at rates comparable to that of TPP-OH. Thus, the conjugates could be used as effective photosensitizers. Furthermore, both conjugates showed higher phototoxicity than TPP-OH, most probably due to their higher intracellular accumulation and sub-cellular localization. However, although TPP–Rh seemed to accumulate predominantly in the mitochondria, TPP–AO accumulated in both the mitochondria and the nucleus. Thus our study suggests that conjugating the Rh moiety to photosensitizers might provide two benefits: enhanced cellular uptake and mitochondrial localization, which are two important subjects in PDT.

4. Experimental section

4.1. General methods

All solvents and reagents were used as obtained from Sigma–Aldrich and Thermo Fisher Scientific unless otherwise stated. All reactions were monitored by TLC using 5–17 μm silica gel plates with fluorescent indicators from Sigma–Aldrich. All column chromatography was done using 40–63 μm silica gel from Sorbent Technologies. NMR spectra were recorded at 25 °C using a Brukner AVANCE 400 Spectrometer. NMR solvents with residual solvent signals were used as internal standards. Elemental analyses were done by Atlantic Microlabs Inc. ESI mass spectrometry was done either at the South Dakota State University Mass Spectrometry Facility or at of the University of Buffalo's Chemistry Department's Instrument Center. Compounds **1**, **2**, and **3** were prepared as described in Refs. 33,34.

4.2. Synthesis

4.2.1. Synthesis of TPP–Rh (4)

The procedure described in a reference was used with several modifications.[35] Briefly, Rh B (127 mg, 2.661 mmol) and K_2CO_3 (735 mg, 0.798 mmol) were added to a solution of porphyrin **3** (200 mg, 0.266 mmol) in acetone (30 mL) and refluxed for 72 h. The reaction mixture was left to cool, then filtered to remove K_2CO_3. The filtrate was next concentrated under reduced pressure, and purified over a silica column using a dichloromethane/methanol (95:5) eluant. A pinkish-purple solid (51%, 152 mg) was obtained. UV–vis (dichloromethane) λ_{max} ($\varepsilon \times 10^3\ M^{-1}\ cm^{-1}$): 419 (389), 522 (37.4), 562 (50.1), 649 (4.7). ^1H NMR (400 MHz, $CDCl_3$): δ 8.84 (8H, s), 8.42 (1H, d, J = 8.0 Hz), 8.21 (6H, d, J = 8.0 Hz), 8.08 (2H, d, J = 8.0), 7.86 (1H, m), 7.75 (10H, m), 7.38 (1H, m), 7.14 (4H, m), 6.93 (1H, d, J = 8.0 Hz), 6.86 (1H, s), 6.81 (1H, d, J = 8.0 Hz), 6.51 (1H, m), 4.42 (2H, m), 4.18 (2H, m), 3.58 (8H, m), 2.17 (2H, m), 1.28 (12H, m), −2.91 (2H, s). ^{13}C NMR (400 MHz, $CDCl_3$): δ 157.64, 155.36, 141.80, 135.34, 134.30, 131.16, 130.39, 127.49, 126.49, 119.93, 113.65, 112.48, 96.04, 64.29, 62.60, 45.70, 30.63, 28.41, 12.07. Low resolution ESI MS: m/z 1113.5 (Calcd for $C_{75}H_{65}N_6O_4^+$ 1113.4); Anal. Calcd for $C_{75}H_{65}Cl_{0.237}I_{0.398}N_6O_4{\cdot}4H_2O$: C, 72.34; H, 5.91; Cl, 0.67; I, 4.01; N, 6.75. Found: C, 73.80; H, 5.39; Cl, 0.73; I, 4.07; N, 6.18.

4.2.2. Synthesis of the 1,3-diiodopropane (5)

1,3-Dibromopropane (5 mL, 49.04 mmol) was added to a solution of KI (488 mg, 147.11 mmol) in 50 mL of acetone. The mixture was then refluxed under nitrogen for 72 h.[36] After this, 30 mL of distilled water was added to the reaction mixture and the product was extracted with 50 mL of diethyl ether. The extracts were combined and washed with 50 mL of distilled water, then dried with Na_2SO_4. The ether was later removed under reduced pressure and the product dried in a vacuum desiccator overnight. The pure product (63%, 8 mL) was obtained as a brown liquid.^1H NMR (400 MHz, $CDCl_3$): δ 3.26 (4H, t, J = 6.4 Hz), 2.24 (2H, m). ^{13}C NMR (400 MHz, $CDCl_3$): δ 35.40, 7.50.

4.2.3. Synthesis of 5,10,15-triphenyl-20-(3-iodopropyl phenyl ether)-21*H*,23*H*-porphyrin (6)

A mixture of porphyrin **(2)** (266 mg, 0.422 mmol), K_2CO_3 (583 mg, 4.22 mmol) and 1,3-diiodopropane (0.63 mL, 0.422 mmol) in 30 mL of acetone was treated as described for compound **3**. A pure purple crystal was obtained (80%, 0.255 mg). ^1H NMR

(400 MHz, $CDCl_3$): δ 8.84 (8H, m), 8.19 (6H, d, J = 8.0 Hz), 8.08 (1H, m, J = 8.0 Hz), 8.00 (1H, d, J = 8.0 Hz), 7.73 (9H, m), 7.22 (1H, m), 7.06 (1H, d, J = 8.0 Hz), 4.25 (2H, m), 3.49 (2H, m), 2.41 (2H, m), −2.91 (2H, s). ^{13}C NMR (400 MHz, $CDCl_3$): δ 158.65, 142.33, 135.77, 134.93, 134.78, 127.84, 126.83, 120.24, 120.15, 113.77, 112.89, 111.61, 67.66, 33.32, 2.83. Low resolution ESI MS: m/z 799.2 (Calcd for $C_{47}H_{36}IN_4O^+$ 799.2).

4.2.4. Synthesis of TPP–AO (7)

A solution of acridine orange base (0.066 mg, 0.2504 mmol) and porphyrin **(6)** (200 mg, 0.2504 mmol) in 5 mL of dry toluene and 2 mL of dimethyl formamide were refluxed for 72 h. The solvent was then removed under reduced pressure and the product purified over a silica column, first with a CH_2Cl_2 eluant until all the unreacted porphyrin was eluted, then with a CH_2Cl_2:CH_3CH_2OH (95:5) eluant. A brownish-orange solid was obtained (54%, 120 mg). UV–vis (dichloromethane) λ_{max} ($\varepsilon \times 10^3$ M^{-1} cm^{-1}): 419 (303.9), 506 (48.2), 553 (7.1), 593 (4.1), 649 (3.7). ^{1}H NMR (400 MHz, $CDCl_3$): δ 8.84 (8H, m), 8.40 (1H, s), 8.15 (9H, m), 7.74 (11H, m), 7.29 (2H, d, J = 8.0 Hz), 6.99 (1H, d), 6.90 (2H, s), 5.15 (2H, m), 4.74 (2H, m), 3.36 (12H, m), 2.65 (2H, s), −2.81 (2H, s). ^{13}C NMR (400 MHz, $CDCl_3$/MeOH): δ 155.48, 142.30, 141.77, 135.78, 134.43, 132.81, 127.72, 126.63, 120.05, 116.56, 113.89, 112.83, 91.89, 78.60, 65.33, 40.52, 31.74, 22.48, 13.83. High resolution ESI MS: m/z 936.4384 (Calcd for $C_{64}H_{54}N_7O^+$ 936.44788); Anal. Calcd for $C_{64}H_{54}IN_7O{\cdot}4H_2O$: C, 67.66; H, 5.50; N, 8.63; I, 11.12. Found: C, 63.48; H, 4.71; N, 7.83; I, 10.14.

4.3. Photophysical properties

4.3.1. Photophysical method

The photophysical properties of the synthesized conjugates and their corresponding components were determined in either dichloromethane, methanol, or dimethyl sulphoxide. Electronic absorption spectra were recorded using either an Ocean Optics Inc. CHEM4-UV-FIBER Spectrophotometer or a Molecular Devices SpectraMax M2 microplate reader. Steady state fluorescence spectra were recorded with either an Edinburgh Instruments F900 fluorescence spectrophotometer equipped with a xenon lamp or with a Molecular Devices SpectraMax M2 microplate reader.

4.3.2. Absorption spectra and molar extinction coefficients

The molar extinction coefficients were calculated from serially diluted solutions. Results were reported in M^{-1} cm^{-1}.

4.3.3. *n*-Octanol/pH 7.4 buffer partition coefficients

n-Octanol/water partition coefficients of the dyes were determined by the 'shake flask' direct measurement method.[37] Saturated solutions of the dyes were prepared by adding the dyes to a mixture of equal volumes (2 mL) of *n*-octanol and a pH 7.4 phosphate buffer. The saturated solutions were placed in an ultrasound bath for 30 min, then left to settle for 4 h. After this, 10 mL of each layer was diluted with dichloromethane and the absorbances of the dyes in the respective solutions determined. The partition coefficients were then obtained by calculating the ratio of the absorbances of the respective dyes in the two layers. Results were reported as log $D_{7.4}$ values.

4.3.4. Aggregation tendency of the dyes

Tendency of the dyes to aggregate in culture media was indirectly determined by comparing their fluorescence intensities in culture medium to that in DMSO.[23] The dyes were dissolved in DMSO (2 mM), diluted to the appropriate concentrations with more DMSO, and 10 μL of the diluted solution added to 190 μL of either complete media or DMSO in 96 well plates to give 10 μM solutions. The plates were then left for an hour after which the fluorescence readings were taken at the appropriate excitation and emission wavelengths. The change in the fluorescence intensities of the dyes in complete media compared to that in DMSO was then used to predict the aggregation tendencies of the dyes. The results were expressed in arbitrary units.

4.3.5. FRET in the conjugates

Decrease in fluorescence intensities of the donor dyes at specific wavelengths, measured in the presence of the acceptor dyes at different distances, was used to demonstrate FRET in the conjugates.[38] A 3D fluorescence scan was used. For each conjugate system, a solution of the conjugate (dyes at close proximity) and an equimolar mixture of the conjugate's individual components (dyes at long range) were compared.

Stock solutions of the dyes (2 mM) were prepared in DMSO. The dye stock solutions were then diluted with methanol to give 1 μM solutions. So, the solutions had not more than 2% (v/v) of DMSO as a cosolvent. For the TPP–Rh system, the fluorescence intensities of a TPP–Rh, solution and an equimolar mixture of TPP-OH and Rh B were used. The solutions were excited every 5 nm from 375 to 550 nm and the fluorescence measured from 555 to 750 nm. While for the TPP–AO system, the fluorescence intensities of a TPP–AO solution and an equimolar mixture of TPP-OH and AO·HCl were excited every 5 nm from 375 to 500 nm and the fluorescence measured from 505 to 750 nm.

In the TPP–Rh system, the decrease in fluorescence intensity of the Rh B peak at 580 nm was used to demonstrate FRET. While in the TPP–AO system, the decrease in the AO·HCl peak at 530 nm was used.

4.3.6. Singlet oxygen generation

The generation of singlet oxygen was determined indirectly, by measuring the rates of oxidation of 1,3-diphenylisobenzofuran (DPBF) by the respective dyes upon irradiation.[39,40] Stock solutions of the respective dyes (2 mM) were prepared in DMSO. A solution of the respective photosensitizer (5 μM) and DPBF (100 μM) in methanol were then prepared in 24 well plates, so that the 2 mL solutions had not more than 2% (v/v) of DMSO as a cosolvent. The well plates were then irradiated using a 60 W Halogen lamp at 0.5 mW cm^{-2} for 10 min. Every 2 min, the absorption readings at 410 nm were taken. The rates (curve slope) of DPBF oxidation by the different dyes were then compared.

4.4. Biological studies

4.4.1. Cells and culture conditions

The rodent mammary adenocarcinoma cell line (R3230AC) was used for all biological experiments. All reagents and culture media were obtained from Invitrogen and Sigma–Aldrich. The cells were maintained in minimum essential medium (α-MEM) supplemented with 10% bovine growth serum, 50 units/mL penicillin G, 50 μg/mL streptomycin and 1.0 μg/mL Fungizone. The cells were incubated at 37 °C in 5% CO_2 using a Sanyo MCO-18AIC-UV incubator. The cells were sub-cultured biweekly to maintain the cells at approximately 80% confluency. The dyes in all studies were initially dissolved in DMSO to make a 2 mM stock solution. A Lab-line Barnstead International orbital shaker was used for all phototoxicity tests and a Molecular Devices SpectraMax M2 microplate reader was used to read UV/Vis absorbances. Either an Edinburgh Instruments F900 spectrophotometer or a Molecular Devices SpectraMax M2 microplate reader was used to read the fluorescence.

4.4.2. Intracellular accumulation

Dye concentrations in cells were determined using the fluorescence intensities of the dyes at appropriate excitation and emission wavelengths, following the procedures in our previous report.[41,42]

4.4.3. Stability of the ester group of TPP–Rh in cells

The cells were seeded at 2.0–3.0 × 10^4 cells/well complete media using 96 well plates and incubated for 24 h. The dye stock solutions were then diluted to the appropriate concentrations with complete media, and added to the cells. The cells were incubated for 24 h after which the medium was removed and the cell monolayer rinsed twice with a 0.9% NaCl solution. DMSO (1900 μL) was then added to dissolve the cells and the fluorescence was read at λ_{ex} = 550 nm and λ_{em} = 650 nm. The fluorescence spectra of TPP–Rh in the cell lysate and in DMSO were then compared. The ratio of the 580 nm and 650 nm fluorescence peaks of TPP–Rh in the cell lysate was also compared to that of TPP–Rh in DMSO.

4.4.4. Sub-cellular localization

Dual staining of each dye with Mitotracker Green (MG, M-7514 from Invitrogen Co.) was tried to determine their mitochondrial localization. Since both TPP-OH and the conjugates (TPP–Rh and TPP–AO) fluoresce in the red region of the optical spectrum, a green filter (Propidium Iodide filter, exciter: HQ535/50; emitter: HQ645/75; set: 41005 from Chroma Technology Co.) was used to acquire the images. For MG which fluoresces in the green region of the optical spectrum, the images were obtained using a red filter (FTC/Bdipy/Fluo3/DiO filter, exciter: HQ480/40; emitter: HQ535/50; set: 41001 from Chroma Technology Co.). However, because some fluorescence from the photosensitizers could be captured with the FTC/Bdipy/Fluo3/DiO (green) filter and some of the fluorescence of Mitotracker Green with the Propidium Iodide filter (red), the exposure time was carefully monitored to avoid/ minimize cross contamination from each other. To determine the appropriate exposure times, the minimum time required to take an image of cells singly stained MG, TPP-OH, TPP–Rh, or TPP–AO were first obtained. The cells were then doubly stained with MG and either TPP-OH, TPP–Rh or TPP–AO and images obtained using both the green and red filters. The green and red images were then superimposed, and the regions of colocalization appeared as yellow.

Cells were seeded at 2.0–3.0 × 10^4 cells/well in 24 well plates containing 12 mm diameter cover slips and then incubated for 24 h. The dyes diluted to the appropriate concentrations were then added to the well plates and incubated for 8 h. After 7 h, 1 μM of Mitotracker Green was added to the cells and the cells incubated for one more hour. After 8 h the media was removed and the cell monolayer rinsed three times with 3 mL of complete media. The cover slide was then mounted on a slide and the images taken using a Leica DMI4000B fluorescence microscope fitted with a QImaging Fast 1394 camera and Qcapture processing software. The images were modified for better visualization with Adobe Photoshop Element 5.0.

4.4.5. Dark toxicity

The cells were treated and cell viability was determined as described in our previous reports.[41,42]

4.4.6. Phototoxicity

The cells were seeded at 1.0–1.5 × 10^4 cells/well in complete media using 96 well plates then incubated for 24 h. The stock solutions of the dyes were then diluted to the appropriate concentrations with complete media and added to the cells. The cells were incubated for 24 h. After this the medium was removed and the cell monolayer rinsed twice with 190 μL of a 0.9% NaCl solution. Clear medium was then added to the wells and the well plate was placed on the well plate shaker. The well plate lids were removed and the wells were exposed to either: (1) broadband visible light delivered at 3 mW cm^{-2} from a 60 W halogen light source for an hour, (2) light delivered at 1.2 mW cm^{-2} from a 630 nm LED source for an hour, or (3) light delivered at 1.2 mW cm^{-2} from a 630 nm LED source for 2 h. The broadband light was filtered through a 3.5 cm water filter (400–850 nm) to prevent heating of the cells. Uniform irradiation of the entire well plate was achieved by gently orbiting the well plate on the shaker. After irradiation, the clear media was removed and 190 μL of complete media added to the wells. The cells were again incubated for 24 h, after which the cytotoxicity was determined by MTT assay and expressed as a percent of the controls (cells exposed to light in the absence of the dyes).

4.4.7. Statistical analyses

Statistical analyses were performed using the Student's *t*-test for pairwise comparisons. A *P* value of <0.05 was considered significant. The Hill (sigmoid E_{max}) equation was fitted to the data to obtain IC_{50} values.

Acknowledgments

This research was supported by the South Dakota Governor's Seed and Competitive Research Grants. We thank Dr. Adam Hoppe for his technical advice in the fluorescence imaging study.

References and notes

1. Detty, M. R. *Exp. Opin. Ther. Pat.* **2001**, *11*, 1849.
2. Sharman, W. M.; Allen, C. M.; van Lier, J. E. *Drug Discovery Today* **1999**, *4*, 507.
3. Kinsella, T. J.; Colussi, V. C.; Oleinick, N. L.; Sibata, C. H. *Exp. Opin. Pharmacother.* **2001**, *2*, 917.
4. Sharman, W. M.; van Lier, J. E.; Allen, C. M. *Adv. Drug Delivery Rev.* **2004**, *56*, 53.
5. Verma, S.; Watt, G. M.; Mai, Z.; Hasan, T. *Photochem. Photobiol.* **2007**, *83*, 996.
6. Macdonald, I. J.; Dougherty, T. J. *J. Porphyrins Phthalocyanines* **2001**, *5*, 105.
7. Dolmans, D. E.; Fukumura, D.; Jain, R. K. *Nat. Rev. Cancer* **2003**, *3*, 380.
8. Shazib, P.; Malini, O. *Clin. Exp. Pharmacol. Physiol.* **2006**, *33*, 551.
9. Castano, A. P.; Demidova, T. N.; Hamblin, M. R. *Photodiag. Photodynam. Ther.* **2004**, *1*, 279.
10. Dougherty, T. J.; Gomer, C. J.; Henderson, B. W.; Jori, G.; Kessel, D.; Korbelik, M.; Moan, J.; Peng, Q. *J. Natl. Cancer Inst.* **1998**, *90*, 889.
11. Rodriguez, M. E.; Azizuddin, K.; Zhang, P.; Chiu, S.; Minh, L.; Malcolm, K. E.; Burda, C.; Oleinick, N. L. *Mitochondrion* **2008**, *8*, 237.
12. Moor, A. C. *J. Photochem. Photobiol., B* **2000**, *57*, 1.
13. Hilf, R. *J. Bioenerg. Biomembr.* **2007**, *39*, 85.
14. Castano, A. P.; Demidova, T. N.; Hamblin, M. R. *Photodiag. Photodynam. Ther.* **2005**, *2*, 1.
15. Dias, N.; Bailly, C. *Biochem. Pharmacol.* **2005**, *70*, 1.
16. Oleinick, N. L.; Morris, R. L.; Belichenko, I. *Photochem. Photobiol. Sci.* **2002**, *1*, 1.
17. Morgan, J.; Oseroff, A. R. *Adv. Drug Delivery Rev.* **2001**, *49*, 71.
18. Modica-Napolitano, J. S.; Aprille, R. J. *Adv. Drug Delivery Rev.* **2001**, *49*, 63.
19. Xu, W.; Chen, H.; Wang, Y.; Zhao, C.; Li, X.; Wang, S.; Weng, Y. *ChemPhysChem* **2008**, *9*, 1409.
20. Wu, J.; Li, N.; Li, K.; Liu, F. *J. Phys. Chem. B* **2008**, *112*, 8134.
21. Chen, Y.; Gryshuk, A.; Achilefu, S.; Ohulchansky, T.; Potter, W.; Zhong, T.; Morgan, J.; Chance, B.; Prasad, P. N.; Henderson, B. W.; Oseroff, A.; Pandey, R. K. *Bioconjugate Chem.* **2005**, *16*, 1264.
22. Mohanty, J.; Nau, M. W. *Angew. Chem., Int. Ed.* **2005**, *44*, 3750.
23. *Photodynamic Tumour Therapy 2nd and 3rd Generation Photosensitizers*; Moser, J. G., Ed.; Harwood Academic: Amsterdam, 1998.
24. Mislick, K. A.; Baldeschwieler, J. D. *Proc. Natl. Acad. Sci.* **1996**, *93*, 12349.
25. Navia, M. A.; Chaturvedi, P. R. *Drug Discovery Today* **1996**, *1*, 179.
26. Satonaka, H.; Kusuzaki, K.; Matsubara, T.; Shintani, K.; Wakabayashi, T.; Nakamura, T.; Matsumine, A.; Uchida, A. *Anticancer Res.* **2007**, *27*, 3339.
27. Kusuzaki, K.; Murata, H.; Matsubara, T.; Miyazaki, S.; Okamura, A.; Seto, M.; Matsumine, A.; Hosoi, H.; Sugimoto, T.; Uchida, A. *Anticancer Res.* **2005**, *25*, 1225.
28. Kusuzaki, K.; Takeshita, H.; Murata, H.; Gebhardt, M.; Springfield, D. S.; Mankin, H. J.; Ashihara, T.; Hirasawa, Y. *Anticancer Res.* **2000**, *20*, 965.
29. Matsubara, T.; Kusuzaki, K.; Matsumine, A.; Shintani, K.; Satonaka, H.; Uchida, A. *Anticancer Res.* **2006**, *26*, 187.
30. Johnson, I. M.; Kumar, S. G.; Malathi, R. J. *Biomol. Struct. Dyn.* **2003**, *20*, 677.
31. Lyles, M. B.; Cameron, I. L. *Biophys. Chem.* **2002**, *96*, 53.
32. Houba-Herin, N.; Calberg-Bacq, C. M.; Van de Vorst, A. *Int. J. Radiat. Biol. Relat. Stud. Phys., Chem. Med. FIELD Full Journal Title: International Journal of Radiation Biology and Related Studies in Physics, Chemistry and Medicine* **1984**, *45*, 487.
33. Banfi, S.; Caruso, E.; Buccafurni, L.; Murano, R.; Monti, E.; Gariboldi, M.; Papa, E.; Gramatica, P. *J. Med. Chem.* **2006**, *49*, 3293.
34. Ouyang, Y.; Peng, Q. *Hecheng Huaxue* **2002**, *10*, 447.
35. Sun, X.; Li, D.; Chen, G.; Zhang, J. *Dyes Pigment* **2006**, *71*, 118.
36. Baughman, T. W.; Sworen, J. C.; Wagener, K. B. *Tetrahedron* **2004**, *60*, 10943.

37. Leo, A.; Hansch, C.; Elkins, D. *Chem. Rev.* **1971**, *71*, 525.
38. Lakowitcz, J. R., Ed. *Principles of Fluorescence Spectroscopy*, 3rd ed., Springer Publishing Company: Chicago, 2006.
39. Spiller, W.; Kliesch, H.; Wöhrle, D.; Hackbarth, S.; Röder, B.; Schnurpfeil, G. *J. Porphyrins Phthalocyanines* **1998**, *2*, 145.
40. Yogo, T.; Urano, Y.; Ishitsuka, Y.; Maniwa, F.; Nagano, T. *J. Am. Chem. Soc.* **2005**, *127*, 12162.
41. Ngen, E. J.; Daniels, T. S.; Murthy, R. S.; Detty, M. R.; You, Y. *Bioorg. Med. Chem.* **2008**, *16*, 3171.
42. You, Y.; Gibson, S. L.; Detty, M. R. *J. Photochem. Photobiol., B* **2006**, *85*, 155.